

Cite this: *Dalton Trans.*, 2019, **48**, 379Received 12th November 2018,
Accepted 26th November 2018

DOI: 10.1039/c8dt04491k

rsc.li/dalton

Dioxygen activation by a dinuclear thiolate-ligated Fe(II) complex†

Chang-Chih Hsieh,^a Yu-Chiao Liu,^b Mei-Chun Tseng,^b Ming-Hsi Chiang ^b and Yih-Chern Horng ^{*a}

Dioxygen activation by Fe^{II} thiolate complexes is relatively rare in biological and chemical systems because the sulfur site is at least as vulnerable as the iron site to oxidative modification. O₂ activation by Fe^{II}–SR complexes with thiolate bound *trans* to the O₂ binding site generally affords the Fe^{IV}=O intermediate and oxidized thiolate. On the other hand, O₂ activation by Fe(II)–SR complexes with thiolate bound *cis* to the O₂ binding site generates Fe^{III}–O–Fe^{III} or *S*-oxygenated complexes. The postulated Fe^{IV}=O intermediate has only been identified in isopenicillin N synthase recently. We demonstrated here that O₂ activation by a dinuclear Fe^{II} thiolate-rich complex produces a mononuclear Fe^{III} complex and water with a supply of electron donors. The thiolate is bound *cis* to the postulated dioxygen binding site, and no Fe^{III}–O–Fe^{III} or *S*-oxygenated complex was observed. Although we have not detected the transient intermediate by spectroscopic measurements, the Fe^{IV}=O intermediate is suggested to exist by theoretical calculation, and *P*-oxidation and hydride-transfer experiments. In addition, an unprecedented Fe^{III}–O₂–Fe^{III} complex supported by thiolates was observed during the reaction by using a coldspray ionization time-of-flight mass (CSI-TOF MS) instrument. This is also supported by low-temperature UV-vis measurements. The intramolecular NH...O=Fe^{IV} hydrogen bonding, calculated by DFT, probably fine tunes the O₂-activation process for intramolecular hydrogen abstraction, avoiding the *S*-oxygenation at *cis*-thiolate.

Introduction

Dioxygen activation for the preparation of an oxidized organic substrate through a redox reaction is generally utilized by iron metalloenzymes.¹ During the catalytic cycles of these enzymes

with a mononuclear active site, Fe-superoxo, -peroxo or high valent oxo complexes have been implicated as reactive intermediates.² In such an oxidizing environment, cysteine (Cys) is thought to be an inappropriate coordinating ligand because the sulfur site is at least as vulnerable as the iron site to oxidative modification. Cytochrome P450 and NO synthase represent the only examples of heme-containing enzymes for the activation of dioxygen with Cys residue ligation.³ In the well-studied cytochrome P450, Cys coordinates axially and facilitates the heterolytic O–O bond cleavage of the Fe^{III}–OOH intermediate to produce an Fe^{IV}=O species.⁴ The other thiolate-ligating Fe enzymes, for example cysteine dioxygenase (CDO)⁵ and isopenicillin N synthase (IPNS),⁶ enable thiolate binding *cis* to the O₂ binding site on the substrate prior to O₂ activation and substrate oxidation. The postulated Fe^{IV}=O catalytic intermediate of these enzymes⁷ was detected in IPNS only recently.⁸ Delicate control over S oxidation is governed by these Fe enzymes, particularly those enzymes with a nonheme active site. There is a lack of thorough understanding, and this is an interesting process to explore. Relatively rare non-heme Fe^{II} thiolate complexes employed for inner-sphere O₂ activation have been reported, where the reaction has only generated *S*-oxygenated⁹ or Fe^{III}–O–Fe^{III} complexes.¹⁰ Besides, whether O₂-mediated generation of *S*-oxygenated products [Fe–S(O)_xR] (*x* = 1, 2, or 3) is Fe(II) based O₂-capture or not still remains elusive.¹¹ Here we report O₂ activation by dinuclear Fe^{II} thiolate-rich complex **1** with NNS ligands (LNHS[–]) in the presence of (LNHS)₂ to produce a mononuclear Fe^{III} complex (**2**), a 1,2-benzisothiazolin-3-one derivative¹² (LN-S), and H₂O (Scheme 1). The reaction mechanism of this process and the observation of an Fe^{III}–O₂–Fe^{III} intermediate are also described.

Experimental

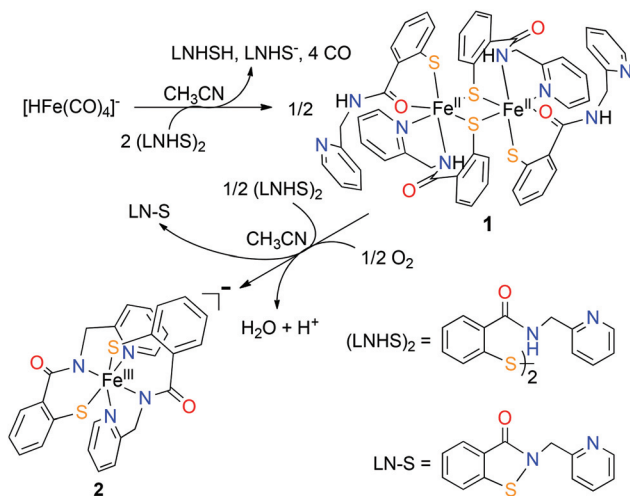
General procedures

Commercially available chemicals were purchased from Aldrich or Acros, and used as received. The organic compound,

^aDepartment of Chemistry, National Changhua University of Education, Changhua 50058, Taiwan. E-mail: ychorng@cc.ncue.edu.tw

^bInstitute of Chemistry, Academia Sinica, Taipei 11528, Taiwan, Republic of China

† Electronic supplementary information (ESI) available: Additional spectroscopic and single-crystal data. CCDC 1838290 (1), 1838291 (2), 1838292 [(LNHS)₂] and 1838293 (LN-S). For ESI and crystallographic data in CIF or other electronic format see DOI: 10.1039/c8dt04491k



Scheme 1 Summary of the reactions for the syntheses of complexes **1**, **2**, LN-S, and reduction of O₂ to H₂O.

2,2'-dithiobenzoyl chloride, was prepared under aerobic conditions.¹³ The inorganic compound [Et₄N][HFe(CO)₄] was synthesized under anaerobic conditions by following the published procedures¹⁴ and stored in a N₂-filled glovebox. The syntheses of iron complexes were performed under a dry nitrogen atmosphere according to standard Schlenk techniques or performed in a glove box. All solvents except for DMSO were distilled, dried, and stored in N₂-filled reservoirs containing 4 Å molecular sieves before use. THF and hexane were distilled under nitrogen using sodium-benzophenone as a drying reagent. Ether and DMF were distilled under nitrogen using CaH₂ as a drying reagent. Dichloromethane was distilled under nitrogen using P₂O₅ as a drying reagent. DMSO was purged under nitrogen and then stored in dried N₂-filled reservoirs containing 4 Å molecular sieves. ¹H, ¹³C and ³¹P NMR spectra were obtained on an Avance 300 spectrometer. Chemical shifts for ¹H and ¹³C{¹H} spectra were recorded in ppm relative to the residual proton and ¹³C of CDCl₃ (¹H: δ 7.24; ¹³C: δ 77.0) and DMSO-d₆ (¹H: δ 2.50; ¹³C: δ 39.5). UV-vis spectra were obtained on a GBC 202 spectrophotometer, while infrared spectra were recorded on a Bruker Alpha instrument using ZnSe discs (0.2 mm, KBr windows). The low-temperature UV-vis spectra were obtained with an Agilent 8453 spectrophotometer. The UV cell was loaded with 0.1 mM of **1** in DMF and cooled to 0 °C or -50 °C, and O₂ was injected to the solution. The coldspray ionization time-of-flight mass (CSI-TOF MS) spectral data were collected on a JMS-T100CS (JEOL) mass spectrometer equipped with a CSI source. Typical measurement conditions are as follows: needle voltage, 0 kV; orifice current, 50–500 nA; orifice voltage, 0 to 20 V; ring lens voltage, 30 V; and spray temperature, -50 °C. EPR spectra were monitored at X-band frequencies by using a Bruker EMS^{plus} spectrometer with an 8" magnet and 2.7 kW power supply. Electrochemical measurements were performed with a CH-611C electrochemical analyzer utilizing 3 mm glassy carbon working, Ag/AgCl reference, and platinum auxiliary

electrodes. Cyclic voltammograms were obtained from solutions containing 1 mM analytes in DMF using 0.1 M [n-Bu₄N][PF₆] as the supporting electrolyte. Elemental analyses and MS spectrometry were performed on a Heraeus CHN-OS Rapid Elemental Analyzer and JEOL JMX-SX/SX 102A Mass Spectrometer at the Instruments Center of National Chung Hsing University, Taiwan.

Synthesis of (LNHS)₂. The synthesis procedure of (LNHS)₂ is the same as the published report.¹⁵ ¹H NMR (300 MHz, d₆-DMSO, 25 °C): δ 9.31 (2H, t), 8.54 (2H, d), 8.03 (2H, d), 7.78 (2H, t), 7.69 (2H, d), 7.48 (2H, t), 7.43 (2H, d), 7.35 (2H, t), 7.28 (2H, t), 4.61 (4H, d). The only product (LNHS)₂ with no trace of LN-S was obtained when LNHS⁻ was stirred in DMSO at 90 °C for 3 h. The air-stable yellow crystals of (LNHS)₂ suitable for X-ray crystallographic analysis were obtained by layering the THF solution with pentane at 4 °C for 1 week.

Preparation of 1. A solution of [Et₄N][HFe(CO)₄] (0.3 g, 1.0 mmol) and (LNHS)₂ (0.97 g, 2.0 mmol) in CH₃CN (20 mL) was stirred at room temperature overnight under a N₂ atmosphere. THF was added to the resulting solution (50 mL) to afford yellow precipitates. The precipitates were collected with a filter, washed with THF (15 mL) three times and dried under vacuum to afford **1** (yield: 0.3 g, 55%). The yield was calculated from the number of Fe moles of [Et₄N][HFe(CO)₄] divided by the number of Fe moles of **1**. The air-unstable yellow crystals of **1** suitable for X-ray crystallographic analysis were obtained by layering the yellow MeCN solution of **1** with ether at room temperature for 1 week. IR (KBr): 3419 (w; ν_{N-H}), 1610, 1525 (s, ν_{C=O}) cm⁻¹; UV/Vis (DMF) [λ_{max}, nm (ε, M⁻¹ cm⁻¹): 361 (18 540); anal. calcd for: C 57.57, H 4.09, N 10.33; found: C 57.70, H 4.46, N 9.95.

Synthesis of 2. A solution of [Et₄N][HFe(CO)₄] (0.31 g, 1.0 mmol) and (LNHS)₂ (1.02 g, 2.1 mmol) in CH₃CN (25 mL) was stirred at room temperature overnight under a N₂ atmosphere. The resulting yellow solution was changed to a dark-green solution immediately by exposure to oxygen. The dark-green solution was further stirred in air for 8 h. The solution was then filtered and concentrated to 10 mL under vacuum and ether (35 mL) was added to precipitate the products. The upper solution was removed using a cannula, and the dark-green precipitates were dried under vacuum to afford **2** (yield: 0.37 g, 66%). The dark-green crystals of **2** suitable for X-ray crystallographic analysis were obtained by layering the MeCN solution with ether at room temperature for 1 week. Alternatively, complex **2** can be obtained from **1** and (LNHS)₂ in CH₃CN. Pure O₂ (2.3 mL, 0.1 mmol) was injected to a solution containing pure **1** (0.11 g, 0.1 mmol) and (LNHS)₂ (0.05 g, 0.1 mmol) in CH₃CN (25 mL) and the solution was stirred at room temperature for 4 h. 20% tetraethylammonium hydroxide aqueous solution (0.15 g, 0.2 mmol) was added to the above solution and stirred for 10 min. The resulting solution was concentrated to 5 mL under vacuum and ether (40 mL) was added to precipitate the products. The upper solution was removed using a cannula, and the dark-green precipitates were dried under vacuum to afford **2** (yield: 0.098 g, 72%). IR (KBr):

1514 (s, $\nu_{\text{C=O}}$) cm^{-1} ; UV/Vis (CH_3CN) [λ_{max} , nm (ϵ , $\text{M}^{-1} \text{cm}^{-1}$): 361 (4370), 454 (1900), 571 (960), 721 (320); anal. calcd for: C 60.27, H 5.98, N 10.65; found: C 60.04, H 5.77, N 10.40.

Synthesis of 2-(pyridin-2-ylmethyl)benzothiazol-3(2H)-one (LN-S). The resulting green solution for the synthesis of complex **2** in DMSO was dried under vacuum at 60 °C to afford a dark green mixture. The dark green powder was dissolved in DMF, and dark green and yellow crystals were obtained by layering the DMF solution with ether at room temperature for 2 weeks. The yellow crystals of LN-S were collected for X-ray crystallographic analysis and other analyses. ^1H NMR (300 MHz, CDCl_3 , 25 °C): δ 8.55 (1H, d), 8.03 (1H, d), 7.62 (1H, t), 7.56 (1H, t), 7.85 (1H, d), 7.36 (1H, t), 7.27 (1H, d), 7.18 (1H, d), 5.14 (2H, s). ^{13}C NMR: δ 165.33, 155.68, 140.57, 137.02, 131.88, 126.71, 125.40, 123.95, 122.86, 122.45, 120.31, 49.00. ^1H NMR (300 MHz, d_6 -DMSO, 25 °C): δ 8.54 (1H, d), 7.96 (1H, d), 7.91 (1H, d), 7.78 (1H, t), 7.68 (1H, t), 7.44 (1H, t), 7.31 (1H, t), 7.29 (1H, d), 5.12 (2H, s). ^{13}C NMR: δ 164.94, 155.03, 147.82, 141.17, 139.68, 132.36, 126.00, 125.86, 123.92, 123.73, 123.08, 122.21, 47.22. IR (KBr): 1658 (s, $\nu_{\text{C=O}}$) cm^{-1} . Anal. calcd for: C 64.44, H 4.16, N 11.56; found: C 64.31, H 3.69, N 11.53.

In situ NMR experiment for complex **1** reacting with oxygen

In a glove-box, a mixture of pure **1** (0.022, 0.02 mmol) and $(\text{LNHS})_2$ (0.010 g, 0.02 mmol) in d_6 -DMSO (15 mL) was stirred at room temperature overnight, and the overnight solution was transferred to a J. Young NMR tube. After collecting the first NMR spectrum of the overnight solution, the J. Young NMR tube was degassed with a vacuum system and filled with oxygen gas to conduct the *in situ* NMR experiment.

In situ NMR experiment for $(\text{LNHS})_2$ reacting with oxygen

A solution of $(\text{LNHS})_2$ (0.003 g) dissolved in d_6 -DMSO (0.4 mL) in air was transferred to a J. Young NMR tube for *in situ* NMR experiment.

Preparation of oxygenated complex **1** for IR measurement

A solution of **1** (0.022 g) in DMF (5 mL) at -50 °C was injected with limited excess O_2 and stirred for 1 min. Ether (50 mL) was added to the green solution to precipitate the oxygenated complex **1**. The upper solution was removed using a cannula, and the green precipitates were collected and dried under vacuum for solid IR experiment.

P-Oxidation experiment

4 equiv. of PPh_3 and 1 equiv. of complex **1** were loaded into a flask prior to adding DMF (20 ml) in a glove box. The mixture in the flask was exposed to air for 20 min, and the solution was transferred to an NMR tube to conduct ^{31}P $\{^1\text{H}\}$ NMR experiment.

Hydride-transfer experiment

4 equiv. of 9,10-dihydroanthracene and 1 equiv. of complex **1** were loaded into a flask prior to adding DCM (20 ml) in a glove box. The mixture in the flask was exposed to air for 30 min, and the solution was loaded into a microtube for high resolution mass spectrometry analysis.

Computational details

DFT calculations were performed on the Gaussian 03 program.¹⁶ Geometry optimizations were conducted using the BP86 functional and 6-31G** basis sets. The spin states of the intermediates **A** and **B**, and complex **1** were assigned as $S = 0$. The spin states of the intermediate **C** and the transition state (**TS**) were assigned as $S = 2$. The spin state of the intermediate **D** was assigned as $S = 1$. The spin states of complex **2** were assigned as $S = 1/2$ supported by EPR measurements.

Crystallography

The crystals suitable for structure analysis were mounted on a glass fiber with silicone grease and placed in the cold stream of a Bruker APEX II with graphite monochromated Mo K_α radiation ($\lambda = 0.71073$ Å) at 150(2) K. All structures were solved by direct methods using SHELXS-97 and refined by full-matrix least squares methods against F^2 with SHELXL-97.¹⁷ Tables of neutral atom scattering factors, f and f' , and absorption coefficients are from a standard source.¹⁸ All atoms except for hydrogen atoms were refined with anisotropic displacement parameters. In general, hydrogen atoms were fixed at calculated positions, and their positions were refined using a riding model. Crystallographic data collection and refinement parameters are given in Table S0.†

Results and discussion

The isolation of **1** was determined based on early reports.¹⁹ Treatment of two equiv. of $(\text{LNHS})_2$ with $[\text{HFe}(\text{CO})_4]^-$ in CH_3CN at RT led to the generation of **1** with the liberation of LNHS and LNHS^- via the formation of the intermediates $[(\text{LNHS})\text{Fe}^0(\text{CO})_4]^-$ and *fac*- $[(\text{LNHS})_3\text{Fe}^{\text{II}}(\text{CO})_3]^-$. Subsequent dimerization occurs with a release of all carbon monoxide moieties. The yellow complex **1** (55% yield) in the solid state is stable for weeks and transforms into a green species gradually within months in air. The crystal structure of **1** was studied using X-ray diffraction, and the molecular structure is shown in Fig. 1 (selected bond lengths and angles in Table S1, ESI†).

Complex **1** has an inversion center in the middle of two metal ions. Each six-coordinated Fe^{II} ion is ligated by two LNHS^- and they are bridged by two thiolato-S donors. Each Fe^{II} ion is coordinated by three thiolato sulfurs, two nitrogens from pyridino and amido moieties, and one carbonyl oxygen. A distal pyridine arm is pointing away from each iron site in both halves of the dimer. The structure of the di-iron(II) core in **1** is significantly different from several reported complexes with similar $\text{Fe}^{\text{II}}-\text{Fe}^{\text{II}}(\mu\text{-SR})_2$ motifs (Table S2, the ESI†).^{10a,20} The relatively long $\text{Fe}\cdots\text{Fe}$ (3.548 Å), short $\text{S}\cdots\text{S}$ (3.490 Å), and long averaged $\text{Fe}-\text{S}_{\text{bridged}}$ (2.488 Å) distances in **1** indicate that complex **1** tends to dissociate into mononuclear fragments in solution. A one-step oxidation or reduction process in cyclic voltammetry analyses (Fig. S1, ESI†) and the detection of monomeric **1** in the coldspray ionization time-of-flight mass (CSI-TOF MS) spectrum (Fig. S11, ESI†) also suggested the existence of mononuclear **1** in solution. Interestingly, hydro-

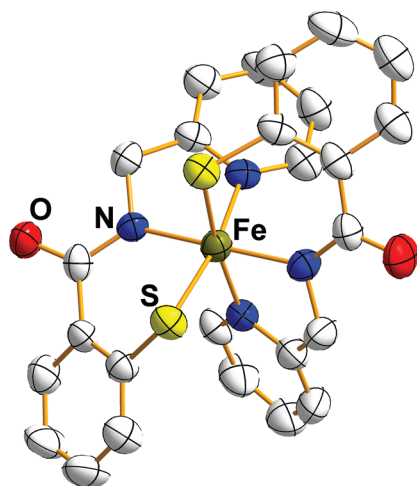
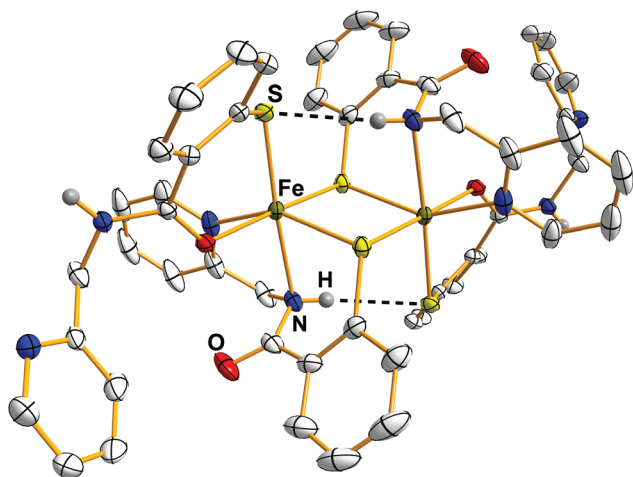


Fig. 1 ORTEP diagrams of **1** (top) and **2** (bottom) with thermal ellipsoids with 50% probability. The NH...S intramolecular hydrogen bond interactions are shown as dashed lines, and the cation in **2** and hydrogen atoms bound to carbon atoms have been omitted for clarity.

gen in the Fe-bound carboxamido NH moiety has an intramolecular NH...S hydrogen bond interaction with the terminal thiolato sulfur bound on the other iron. The N...S contact distance of 3.379 Å is comparable to those of other complexes with hydrogen-bond interactions.²¹ In addition, the intermolecular NH...N hydrogen bond interactions utilizing carboxamido NH and pyridino nitrogen on the distal pyridine arm were revealed to occur between molecules forming the 1D polymer (Fig. S2, ESI†).

Interestingly, when a solution containing pure **1** and one equiv. of (LNHS)₂ was exposed to oxygen in CH₃CN, the solution color changed immediately from yellow to dark-green. **2** was isolated from the solution with 72% yield. Due to the low solubility of **1** in CH₃CN, the studies of the reaction process during the transformation of **1** into **2** were performed in DMSO or DMF. The reaction of **1** and limited O₂ in the presence of (LNHS)₂ in DMSO shows no trace of *S*-oxygenation pro-

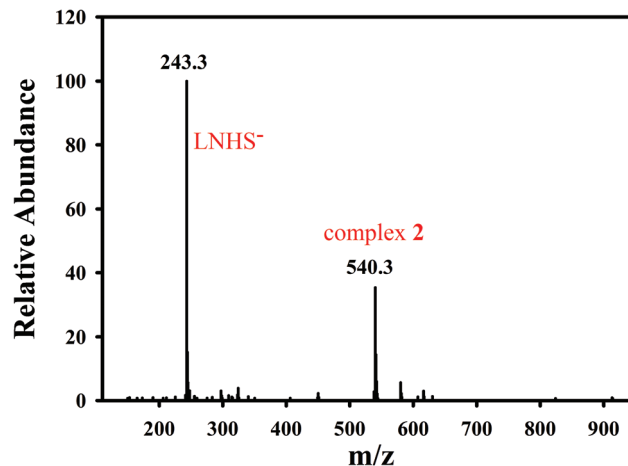


Fig. 2 ESI-MS spectrum of the solution containing pure **1** and one equiv. of (LNHS)₂ exposed to oxygen for synthesizing complex **2** in DMSO.

ducts as determined by electrospray ionization mass spectrometry (ESI-MS) (Fig. 2). However, **1** without adding (LNHS)₂ in DMSO supplied with a slight excess of O₂ consecutively for at least 2 h at RT afforded EPR-silent species. The initial green solution gradually turned yellow with the detection of LNHSO₃⁻ (*m/z* 291.0) and no trace of **2** by ESI-MS after 5 h (Fig. 3). Therefore, the organic ligand (LNHS)₂ must exist for the formation of **2** during the reaction between **1** and O₂. The molecular structure of **2** (Fig. 1, bottom) was obtained successfully and the selected bond lengths and angles are listed in Table S3, ESI.† Two similar Fe-S, Fe-N(amido) or Fe-N(pyridino) bond distances indicate that the two ligands contribute to the electron density equally on the iron ion. The hydrogens of the carboxamido NH moieties disappeared in **2**. The X-band EPR spectrum of **2** in 50% DMSO aqueous solution at 77 K displays an axial signal with *g* values at 2.19 and 1.95 (Fig. S3, the ESI†), indicating the low-spin nature of the Fe^{III} center with an asymmetric coordination environment in solution. The

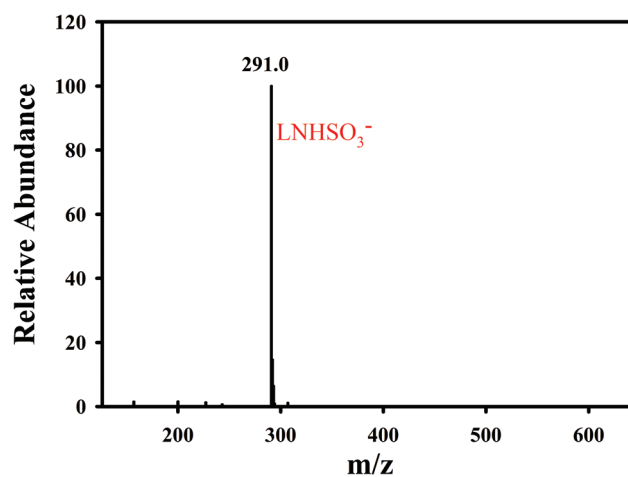


Fig. 3 ESI-MS spectrum of pure **1** without adding (LNHS)₂ reacted with a slight excess of O₂ in DMSO for 5 h.

$\text{Fe}^{\text{III}}\text{-O-Fe}^{\text{III}}$ or *S*-oxygenated species that were observed in the similar O_2 -activation by $\text{Fe}^{\text{II}}\text{-SR}$ complexes were not found in the O_2 -activation by **1**.

The *in situ* ^1H NMR experiments in d_6 -DMSO were employed to monitor the reaction process during the transformation of **1** into **2** in the presence of $(\text{LNHS})_2$. The chemical shifts of pure complexes **1** and **2** were not observed in d_6 -DMSO due to the inherent paramagnetism. Therefore, the peaks that appeared in the *in situ* ^1H NMR spectra correspond to the chemicals without Fe complexes. As expected, the initial reaction mixture contained mostly $(\text{LNHS})_2$ before being exposed to dioxygen. After the reaction proceeded for 2 h, the intensity of the peak corresponding to the chemical shift of water (δ 3.40 ppm) increased with time, and the intensity of the chemical shifts corresponding to $(\text{LNHS})_2$ (CH_2 at δ 4.60 ppm) decreased with the generation of a benzisothiazol-3(2*H*)-one derivative (LN-S, CH_2 at δ 5.11 ppm) simultaneously (Fig. S4, ESI †). It was known that $(\text{LNHS})_2$ or LNHS cannot be oxidized in DMSO to generate LN-S even in the presence of oxygen with 90 °C reflux for 5 days (see Fig. S5, ESI †). The X-ray structures of $(\text{LNHS})_2$ and LN-S are shown in Fig. S6, ESI †). Thus, from the ^1H NMR experiments, $(\text{LNHS})_2$ acts as an electron donor driving the reaction of **1** and O_2 to form **2** and H_2O . Without the addition of $(\text{LNHS})_2$, the reaction product of **1** and O_2 gradually decomposed and *S*-oxygenated species were formed as evidenced by the detection of LNHSO_3^- .

The delay of LN-S formation (~ 5 h) during the O_2 activation process using pure **1** and $(\text{LNHS})_2$ in DMSO at RT provides an opportunity to explore the nature of possible intermediates. Actually, pure **1** in DMSO supplied with a slight excess of O_2 in the presence of 5 equiv. of ferrocene produced **2** within 1 min, which was confirmed by EPR (Fig. 4). This implies that the electron-transfer reaction is the rate-limiting step for the production of H_2O and **2**. In good correlation with the EPR results, UV-vis spectra revealed that **1** with and without $(\text{LNHS})_2$ in DMSO reacting with O_2 initially yielded the same

transient green species with a half-life of 2.5 and 5 h at RT, respectively. It is known that the typical metal-bound sulfinate ($-\text{SO}_2$) and sulfonate ($-\text{SO}$) stretches are in the range of $1000\text{--}1150\text{ cm}^{-1}$ ^{19d,22} and $900\text{--}1000\text{ cm}^{-1}$,²³ respectively. This green species show no obvious peak corresponding to sulfur oxidation in either range from solid IR measurements (Fig. S7, ESI †). Thus, the possibility of this species derived from the *S*-oxygenated reaction can be exclusively ruled out. As shown in Fig. 5, the reaction of **1** with a slight excess of O_2 led to the appearance of three new absorption bands at $\lambda_{\text{max}} = 460\text{ nm}$, 570 nm, and 670 nm for the green species, and they decayed gradually after 20 h. The reactivity of **1** with O_2 at $-50\text{ }^\circ\text{C}$ nearly mirrored that at RT except for the apparent absorption at 730 nm, and this green chromophore ($\lambda_{\text{max}} = 570\text{ nm}$, and 730 nm) was stable for at least 5 h at this low temperature (Fig. 6). The absorption band with λ_{max} at 570 nm ($\epsilon \sim 2300\text{ M}^{-1}\text{ cm}^{-1}$) is assigned to

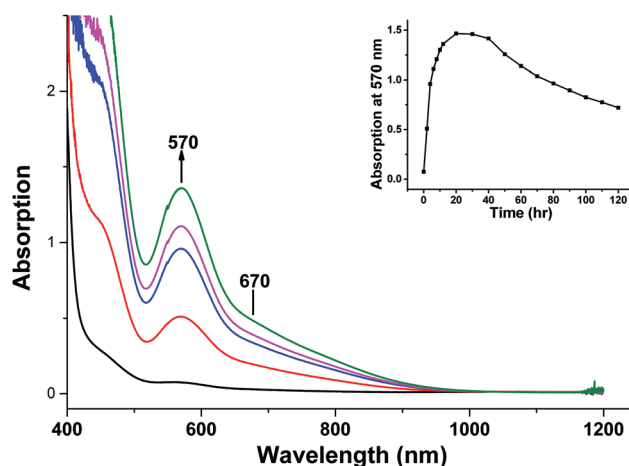


Fig. 5 UV-vis spectral changes for the reaction of **1** with a limited excess of O_2 in DMSO at RT, leading to the formation of an $\text{Fe}^{\text{III}}\text{-O}_2\text{-Fe}^{\text{III}}$ intermediate. The inset shows the time-dependent increase and decrease of the absorption band at 570 nm. The decaying curves are shown in Fig. S8, ESI † .

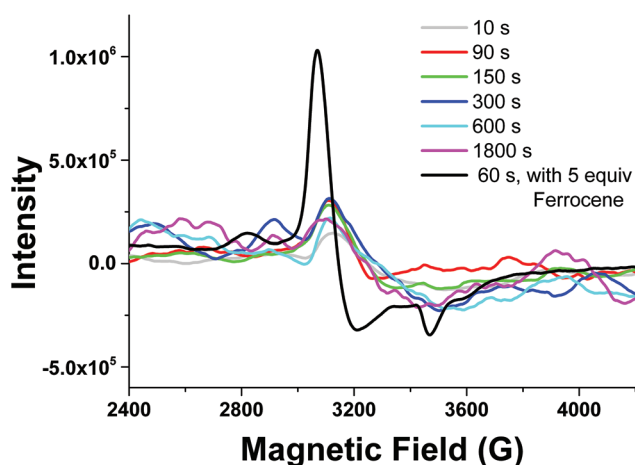


Fig. 4 X-band EPR spectra of pure **1** in DMSO after adding an excess of O_2 at various time points in the absence and presence of ferrocene at room temperature.

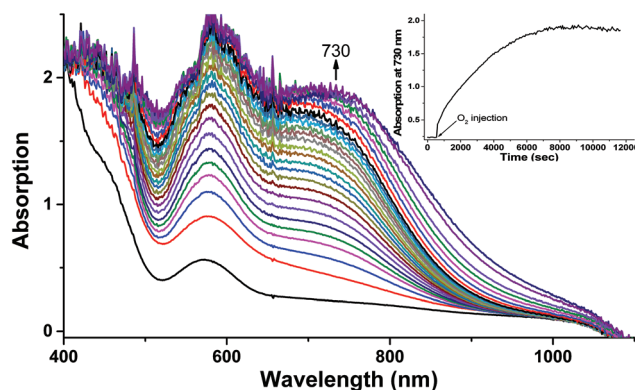


Fig. 6 UV-vis spectral changes for the reaction of **1** with a limited excess of O_2 in DMF at $-50\text{ }^\circ\text{C}$, leading to the formation of an $\text{Fe}^{\text{III}}\text{-O}_2\text{-Fe}^{\text{III}}$ intermediate. The inset shows the time-dependent increase of the absorption band at 730 nm.

the sulfur-to-Fe(III) charge transfer band and the one with λ_{max} at 730 nm ($\epsilon \sim 1900 \text{ M}^{-1} \text{ cm}^{-1}$) is very similar to those observed in the reported $\text{Fe}^{\text{III}}\text{-O}_2\text{-Fe}^{\text{III}}$ complexes with N- and O-based ligands.²⁴ CSI-TOF MS analysis at $-50 \text{ }^\circ\text{C}$ also suggested the formation of an $\text{Fe}^{\text{III}}\text{-O}_2\text{-Fe}^{\text{III}}$ product, as shown by the peak at m/z 1139 (Fig. S9, ESI†). The HRMS data along with the isotopic distribution pattern (Fig. S10, ESI†) can correspond to an ion with the composition of $[1 + \text{O}_2 + \text{Na}]^+$, identical to the $\text{Fe}^{\text{III}}\text{-O}_2\text{-Fe}^{\text{III}}$ intermediate with the sodium ion. To our knowledge, this is the first time the $\text{Fe}^{\text{III}}\text{-O}_2\text{-Fe}^{\text{III}}$ complex with thiolate ligation is detected. Attempts to obtain suitable crystals of the green species for X-ray characterization have been unsuccessful so far.

To detect other intermediates in the **1**-mediated O_2 activation process, the oxygenation of **1** was conducted in the presence of ferrocene at $0 \text{ }^\circ\text{C}$ and monitored using a UV-vis spectrometer. However, no new peak can be obviously observed except for the formation of **2** (Fig. 7). *P*-Oxidation, *S*-oxidation and hydride-transfer experiments using PPh_3 , PhSMe , and 9,10-dihydroanthracene, respectively, were conducted to test the existence of the intermediate with the $\text{Fe}^{\text{IV}}=\text{O}$ functional group in the reaction process.^{2d,25} This green species converted 30% PPh_3 to $\text{O}=\text{PPh}_3$ after 20 min (Fig. S12, ESI†) and anthracene was detected by high resolution mass spectrometry (HRMS) after 30 min (Fig. S13, ESI†). However, the green species did not react at all with MeSPh at RT. The results indicate the involvement of an Fe^{IV} oxo species in the oxygenation process. The $\text{Fe}^{\text{IV}}=\text{O}$ intermediate is probably too transient to be detected using an UV-vis spectrometer at $0 \text{ }^\circ\text{C}$.

In order to gain insight into the reaction process, density functional theory (DFT) calculation was used to examine the possible candidates. The optimized geometries of the two Fe^{III} intermediates with two oxygen atoms (**A**: end-on conformation; **B**: side-on conformation) were initially evaluated, and the iron^{IV}-oxo (**C**) and iron^{IV}-hydroxide (**D**) intermediates, as well

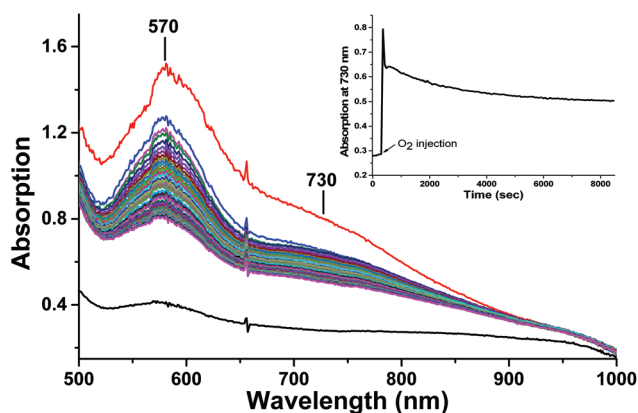
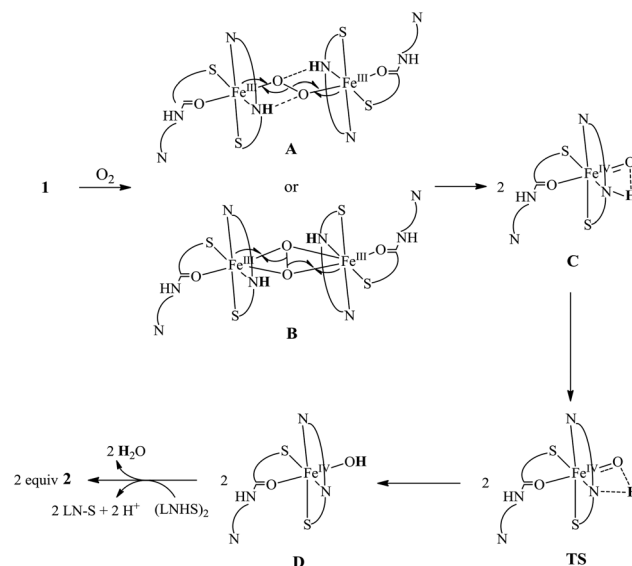


Fig. 7 Time-dependent UV-vis spectra of oxygenation of **1** in the presence of two equiv. of ferrocene in DMF at $0 \text{ }^\circ\text{C}$ (pure **1**: black line; the first time point of **1** exposed to O_2 : red line). After the addition of oxygen to **1**, the absorption bands at 570 and 730 nm were increased immediately and decreased by time to form **2**. The inset shows the time-dependent increase and decrease of the absorption band at 730 nm.



Scheme 2 Proposed reaction mechanism for O_2 activation by **1**.

as the transition state (**TS**), were also calculated. The reaction mechanism (Scheme 2) and the energy diagram (Fig. 8) are shown. The mononuclear Fe^{II} resulting from the partial dissociation of dimeric **1** provides a vacant site for oxygen binding,²⁶ and an O_2 molecule can insert into the di-iron(II) core of **1** to form **A** or **B**. The intermediate **A** ($-43.8 \text{ kcal mol}^{-1}$) is more energy-favorable than **B** ($-4.5 \text{ kcal mol}^{-1}$). It is interesting to note that the oxygen atoms of the bound peroxide in **A** have intramolecular hydrogen bond interactions with the hydrogens of the coordinated carboxamido NH groups (Fig. S14, ESI†). The $\text{Fe}^{\text{IV}}=\text{O}$ intermediate **C** is generated further by homolytic cleavage of the O-O peroxide bond. Although there are rare examples of $\text{Fe}^{\text{IV}}\text{-OH}$ species in the nonheme system reported,²⁷ **D** with an $\text{Fe}^{\text{IV}}\text{-OH}$ group ($-80.7 \text{ kcal mol}^{-1}$) is more stable than **C** ($-51.8 \text{ kcal mol}^{-1}$) in

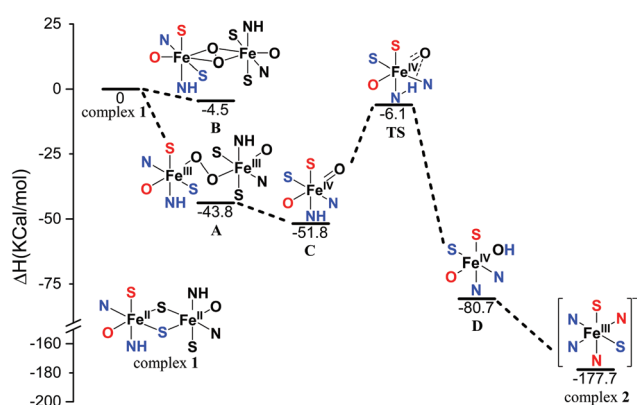


Fig. 8 BP86/6-31G** free-energy profile for oxygen activation from complex **1** to form complex **2** and water. All structures are simplified as Fe atom with bonded atoms, and the atoms with different colors indicate that the atoms belong to different ligands.

our DFT calculation results. The carboxamido hydrogen in close contact with the oxygen in the $\text{Fe}^{\text{IV}}=\text{O}$ motif facilitates the formation of **D** by intramolecular hydrogen transfer, and this prediction was supported by the low activation energy of the **TS** (Fig. S15, ESI[†]). Thus, hydrogen bonding in $\text{NH}\cdots\text{O}=\text{Fe}^{\text{IV}}$ favors intramolecular hydrogen abstraction and avoids *S*-oxygenation at *cis*-thiolate.²⁸ Consecutively, after the hydroxyl group of intermediate **D** abstracts a proton in the unbound amide to form water dissociated from iron, and the Fe^{IV} center obtains an electron from the organic ligand $(\text{LNHS})_2$, **2** is formed by structural rearrangement.

Conclusions

In conclusion, we have shown that a dimeric Fe^{II} complex with NNS chelating ligands, $\text{Fe}_2(\text{LNHS})_4$ (**1**), is capable of activating dioxygen through an inner-sphere mechanism to form water with a supply of electron donors. Although the crystal structure has not been obtained, the $\text{Fe}^{\text{III}}-\text{O}_2-\text{Fe}^{\text{III}}$ species is detected to be the essential intermediate during the reaction. In addition, the Fe^{IV} oxo species is suggested as a transient intermediate evidenced by *P*-oxidation and hydride-transfer experiments. Under limited excess O_2 conditions, the intramolecular $\text{NH}\cdots\text{O}=\text{Fe}^{\text{IV}}$ hydrogen bonding probably fine tunes the O_2 -activation process, thus avoiding *S*-oxygenation at *cis*-thiolate.

Conflicts of interest

There are no conflicts to declare.

Acknowledgements

We gratefully acknowledge the financial support from the Ministry of Science and Technology of Taiwan (MOST 106-2113-M-018-007 to Y.-C. H.).

Notes and references

- (a) C. E. Tinberg and S. J. Lippard, *Acc. Chem. Res.*, 2011, **44**, 280–288; (b) K. Ray, F. F. Pfaff, B. Wang and W. Nam, *J. Am. Chem. Soc.*, 2014, **136**, 13942–13958; (c) A. J. Jasiewicz and L. Que Jr., *Chem. Rev.*, 2018, **118**, 2554–2592; (d) X. Huang and J. T. Groves, *Chem. Rev.*, 2018, **118**, 2491–2553.
- (a) J. T. Groves, *J. Inorg. Biochem.*, 2006, **100**, 434–447; (b) C. Krebs, D. Galonić Fujimori, C. T. Walsh and J. M. Bollinger, *Acc. Chem. Res.*, 2007, **40**, 484–492; (c) E. G. Kovaleva, M. B. Neibergall, S. Chakrabarty and J. D. Lipscomb, *Acc. Chem. Res.*, 2007, **40**, 475–483; (d) W. Nam, Y.-M. Lee and S. Fukuzumi, *Acc. Chem. Res.*, 2014, **47**, 1146–1154.
- Y. Zhu and R. B. Silverman, *Biochemistry*, 2008, **47**, 2231–2243.
- (a) I. Schlichting, J. Berendzen, K. Chu, A. M. Stock, S. A. Maves, D. E. Benson, R. M. Sweet, D. Ringe, G. A. Petsko and S. G. Sligar, *Science*, 2000, **287**, 1615–1622; (b) K. Auclair, P. Moëne-Loccoz and P. R. Ortiz de Montellano, *J. Am. Chem. Soc.*, 2001, **123**, 4877–4885.
- (a) J. G. McCoy, L. J. Bailey, E. Bitto, C. A. Bingman, D. J. Aceti, B. G. Fox and G. N. Phillips Jr., *Proc. Natl. Acad. Sci. U. S. A.*, 2006, **103**, 3084–3089; (b) C. R. Simmons, Q. Liu, Q. Huang, Q. Hao, T. P. Begley, P. A. Karplus and M. H. Stipanuk, *J. Biol. Chem.*, 2006, **281**, 18723–18733.
- (a) P. L. Roach, I. J. Clifton, V. Fulop, K. Harlos, G. J. Barton, J. Hajdu, I. Andersson, C. J. Schofield and J. E. Baldwin, *Nature*, 1995, **375**, 700–704; (b) W. A. Schenk, *Angew. Chem., Int. Ed.*, 2000, **39**, 3409–3411.
- (a) P. L. Roach, I. J. Clifton, C. M. H. Hensgens, N. Shibata, C. J. Schofield, J. Hajdu and J. E. Baldwin, *Nature*, 1997, **387**, 827–830; (b) N. I. Burzlaff, P. J. Rutledge, I. J. Clifton, C. M. H. Hensgens, M. Pickford, R. M. Adlington, P. L. Roach and J. E. Baldwin, *Nature*, 1999, **401**, 721–724; (c) S. Ye, X. A. Wu, L. Wei, D. Tang, P. Sun, M. Bartlam and Z. Rao, *J. Biol. Chem.*, 2007, **282**, 3391–3402; (d) W. Ge, I. J. Clifton, J. E. Stok, R. M. Adlington, J. E. Baldwin and P. J. Rutledge, *J. Am. Chem. Soc.*, 2008, **130**, 10096–10102; (e) D. Kumar, W. Thiel and S. P. de Visser, *J. Am. Chem. Soc.*, 2011, **133**, 3869–3882; (f) E. P. Tchesnokov, A. S. Faponle, C. G. Davies, M. G. Quesne, R. Turner, M. Fellner, R. J. Souness, S. M. Wilbanks, S. P. de Visser and G. N. Jameson, *Chem. Commun.*, 2016, **52**, 8814–8817.
- E. Tamanaha, B. Zhang, Y. Guo, W. C. Chang, E. W. Barr, G. Xing, J. St Clair, S. Ye, F. Neese, J. M. Bollinger Jr. and C. Krebs, *J. Am. Chem. Soc.*, 2016, **138**, 8862–8874.
- (a) D. Sellmann, S. Y. Shaban and F. W. Heinemann, *Eur. J. Inorg. Chem.*, 2004, **2004**, 4591–4601; (b) Y. Jiang, L. R. Widger, G. D. Kasper, M. A. Siegler and D. P. Goldberg, *J. Am. Chem. Soc.*, 2010, **132**, 12214–12215; (c) Y. M. Badiei, M. A. Siegler and D. P. Goldberg, *J. Am. Chem. Soc.*, 2011, **133**, 1274–1277; (d) A. C. McQuilken, Y. Jiang, M. A. Siegler and D. P. Goldberg, *J. Am. Chem. Soc.*, 2012, **134**, 8758–8761; (e) M. Sallmann, I. Siewert, L. Fohlmeister, C. Limberg and C. Knispel, *Angew. Chem., Int. Ed.*, 2012, **51**, 2234–2237; (f) M. Sallmann and C. Limberg, *Acc. Chem. Res.*, 2015, **48**, 2734–2743; (g) A. A. Fischer, N. Stracey, S. V. Lindeman, T. C. Brunold and A. T. Fiedler, *Inorg. Chem.*, 2016, **55**, 11839–11853.
- (a) G. Musie, C.-H. Lai, J. H. Reibenspies, L. W. Sumner and M. Y. Darensbourg, *Inorg. Chem.*, 1998, **37**, 4086–4093; (b) R. M. Theisen, J. Shearer, W. Kaminsky and J. A. Kovacs, *Inorg. Chem.*, 2004, **43**, 7682–7690; (c) S. Ohta, S. Yokozawa, Y. Ohki and K. Tatsumi, *Inorg. Chem.*, 2012, **51**, 2645–2651.
- (a) A. C. McQuilken and D. P. Goldberg, *Dalton Trans.*, 2012, **41**, 10883–10899; (b) G. Villar-Acevedo, P. Lugo-Mas, M. N. Blakely, J. A. Rees, A. S. Ganas, E. M. Hanada, W. Kaminsky and J. A. Kovacs, *J. Am. Chem. Soc.*, 2017, **139**, 119–129.
- T. Li, L. Yang, K. Ni, Z. Shi, F. Li and D. Chen, *Org. Biomol. Chem.*, 2016, **14**, 6297–6303.

- 13 A. Sadeghian, S. M. Seyedi, H. Sadeghian, A. Hazrathoseyni and M. Sadeghian, *J. Sulfur Chem.*, 2007, **28**, 597–605.
- 14 I. Y. Guzman-Jimenez, J. W. van Hal and K. H. Whitmire, *Organometallics*, 2003, **22**, 1914–1922.
- 15 T. C. Harrop, M. M. Olmstead and P. K. Mascharak, *Inorg. Chem.*, 2005, **44**, 9527–9533.
- 16 M. J. Frisch, G. W. Trucks, H. B. Schlegel, G. E. Scuseria, M. A. Robb, J. R. Cheeseman, J. A. Montgomery, T. Vreven, K. N. Kudin, J. C. Burant, J. M. Millam, S. S. Iyengar, J. Tomasi, V. Barone, B. Mennucci, M. Cossi, G. Scalmani, N. Rega, G. A. Petersson, H. Nakatsuji, M. Hada, M. Ehara, K. Toyota, R. Fukuda, J. Hasegawa, M. Ishida, T. Nakajima, Y. Honda, O. Kitao, H. Nakai, M. Klene, X. Li, J. E. Knox, H. P. Hratchian, J. B. Cross, V. Bakken, C. Adamo, J. Jaramillo, R. Gomperts, R. E. Stratmann, O. Yazyev, A. J. Austin, R. Cammi, C. Pomelli, J. W. Ochterski, P. Y. Ayala, K. Morokuma, G. A. Voth, P. Salvador, J. J. Dannenberg, V. G. Zakrzewski, S. Dapprich, A. D. Daniels, M. C. Strain, O. Farkas, D. K. Malick, A. D. Rabuck, K. Raghavachari, J. B. Foresman, J. V. Ortiz, Q. Cui, A. G. Baboul, S. Clifford, J. Cioslowski, B. B. Stefanov, G. Liu, A. Liashenko, P. Piskorz, I. Komaromi, R. L. Martin, D. J. Fox, T. Keith, A. Laham, C. Y. Peng, A. Nanayakkara, M. Challacombe, P. M. W. Gill, B. Johnson, W. Chen, M. W. Wong, C. Gonzalez, J. A. Pople, *Gaussian 03, Revision C.02*, Gaussian, Inc., Wallingford, CT 2004.
- 17 G. M. Sheldrick, *SHELXTL, Version 5.1*, Bruker AXS Inc., Madison, WI, 1998.
- 18 L. E. Sutton, *Tables of Interatomic Distances and Configurations in Molecules and Ions*, Chemical Society Publications, UK, 1965.
- 19 (a) W.-F. Liaw, C.-H. Chen, G.-H. Lee and S.-M. Peng, *Organometallics*, 1998, **17**, 2370–2372; (b) W.-F. Liaw, J.-H. Lee, H.-B. Gau, C.-H. Chen and G.-H. Lee, *Inorg. Chim. Acta*, 2001, **322**, 99–105.
- 20 (a) W.-J. Hu and S. J. Lippard, *J. Am. Chem. Soc.*, 1974, **96**, 2366–2372; (b) D. K. Mills, Y. M. Hsiao, P. J. Farmer, E. V. Atnip, J. H. Reibenspies and M. Y. Darensbourg, *J. Am. Chem. Soc.*, 1991, **113**, 1421–1423; (c) D. Sellmann, J. Utz and F. W. Heinemann, *Inorg. Chem.*, 1999, **38**, 459–466; (d) P. Ghosh, A. Begum, E. Bill, T. Weyhermüller and K. Wieghardt, *Inorg. Chem.*, 2003, **42**, 3208–3215; (e) D. Sellmann, K. P. Peters and F. W. Heinemann, *Eur. J. Inorg. Chem.*, 2004, **2004**, 581–590.
- 21 (a) K.-Y. Wu, C.-C. Hsieh and Y.-C. Horng, *J. Organomet. Chem.*, 2009, **694**, 2085–2091; (b) E. M. Gale, B. S. Narendrapurapu, A. C. Simmonett, H. F. Schaefer and T. C. Harrop, *Inorg. Chem.*, 2010, **49**, 7080–7096.
- 22 (a) C. S. A. Masitas, M. Kumar, M. S. Mashuta, P. M. Kozlowski and C. A. Grapperhaus, *Inorg. Chem.*, 2010, **49**, 10875–10881; (b) E. Galardon, M. Giorgi and I. Artaud, *Chem. Commun.*, 2004, 286–287; (c) C.-M. Lee, C.-H. Hsieh, A. Dutta, G.-H. Lee and W.-F. Liaw, *J. Am. Chem. Soc.*, 2003, **125**, 11492–11493; (d) L. A. Tyler, J. C. Noveron, M. M. Olmstead and P. K. Mascharak, *Inorg. Chem.*, 1999, **38**, 616–617.
- 23 (a) P. Lugo-Mas, A. Dey, L. Xu, S. D. Davin, J. Benedict, W. Kaminsky, K. O. Hodgson, B. Hedman, E. I. Solomon and J. A. Kovacs, *J. Am. Chem. Soc.*, 2006, **128**, 11211–11221; (b) T. Yano, Y. Wasada-Tsutsui, H. Arii, S. Yamaguchi, Y. Funahashi, T. Ozawa and H. Masuda, *Inorg. Chem.*, 2007, **46**, 10345–10353; (c) C. A. Grapperhaus and M. Y. Darensbourg, *Acc. Chem. Res.*, 1998, **31**, 451–459.
- 24 (a) A. Mukherjee, M. A. Cranswick, M. Chakrabarti, T. K. Paine, K. Fujisawa, E. Münck and L. Que, *Inorg. Chem.*, 2010, **49**, 3618–3628; (b) K. Kim and S. J. Lippard, *J. Am. Chem. Soc.*, 1996, **118**, 4914–4915; (c) N. Kitajima, N. Tamura, H. Amagai, H. Fukui, Y. Moro-oka, Y. Mizutani, T. Kitagawa, R. Mathur and K. Heerwegh, *J. Am. Chem. Soc.*, 1994, **116**, 9071–9085.
- 25 C. E. MacBeth, A. P. Golombek, V. G. Young, C. Yang, K. Kuczera, M. P. Hendrich and A. S. Borovik, *Science*, 2000, **289**, 938–941.
- 26 S. Menage, B. A. Brennan, C. Juarez-Garcia, E. Munck and L. Que, *J. Am. Chem. Soc.*, 1990, **112**, 6423–6425.
- 27 (a) T. A. Jackson, J.-U. Rohde, M. S. Seo, C. V. Sastri, R. DeHont, A. Stubna, T. Ohta, T. Kitagawa, E. Münck, W. Nam and L. Que, *J. Am. Chem. Soc.*, 2008, **130**, 12394–12407; (b) A. T. Fiedler and L. Que Jr., *Inorg. Chem.*, 2009, **48**, 11038–11047.
- 28 D. C. Lacy, R. Gupta, K. L. Stone, J. Greaves, J. W. Ziller, M. P. Hendrich and A. S. Borovik, *J. Am. Chem. Soc.*, 2010, **132**, 12188–12190.